Spatiotemporal analysis for detection of pre-symptomatic shape changes in neurodegenerative diseases: Initial application to the GENFI cohort

Claire Cury [a,b,*], Stanley Durrleman [d], David M. Cash [a,b], Marco Lorenzi [a,e], Jennifer M. Nicholas [b,f], Martina Bocchetta [b], John C. van Swieten [g], Barbara Borroni [h], Daniela Galimberti [i], Mario Masellis [j], Maria Carmela Tartaglia [k], James B. Rowe [l], Caroline Graff [m,n,o], Fabrizio Tagliavini [p], Giovanni B. Frisoni [q], Robert Laforce Jr. [r], Elizabeth Finger [s], Alexandre de Mendonça [t], Sandro Sorbi [u,v], Sebastien Ourselin [a,b,c], Jonathan D. Rohrer [b], Marc Modat [a,b,c], on behalf of theGenetic FTD Initiative, GENFI[1]

[a] Department of Medical Physics and Biomedical Engineering, University College London, United Kingdom
[b] Dementia Research Centre, UCL Queen Square Institute of Neurology, University College of London, WC1N 3BG, London, United Kingdom
[c] School of Biomedical Engineering and Imaging Sciences, King's College London, United Kingdom
[d] Inria Aramis Project-team Centre Paris-Rocquencourt, Inserm U 1127, CNRS UMR 7225, Sorbonne Universités, UPMC Univ Paris 06 UMR S 1127, Institut du Cerveau et de la Moelle épinière, ICM, F-75013, Paris, France
[e] Epione Team, Inria Sophia Antipolis, Sophia Antipolis, France
[f] Department of Medical Statistics, London School of Hygiene & Tropical Medicine, London, United Kingdom
[g] Erasmus Medical Center, Rotterdam, the Netherlands
[h] University of Brescia, Italy
[i] Dept. of Pathophysiology and Transplantation, "Dino Ferrari" Center, University of Milan, Fondazione C Granda, IRCCS Ospedale Maggiore Policlinico, Milan, Italy
[j] Cognitive Neurology Research Unit, Sunnybrook Health Sciences Centre, Hurvitz Brain Sciences Research Program, Sunnybrook Research Institute, Department of Medicine, University of Toronto, Canada
[k] Tanz Centre for Research in Neurodegenerative Diseases, University of Toronto, Canada
[l] University of Cambridge, United Kingdom
[m] Karolinska Institutet, Stockholm, Sweden
[n] Karolinska Institutet, Department NVS, Center for Alzheimer Research, Division of Neurogeriatrics, Sweden
[o] Department of Geriatric Medicine, Karolinska University Hospital, Stockholm, Sweden
[p] Instituto Neurologico Carlo Besta, Milan, Italy
[q] IRCCS San Giovanni di Dio Fatebenefratelli Brescia, Italy
[r] Université Laval, Quebec, Canada
[s] University of Western Ontario, Ontario, Canada
[t] Faculdade de Medicina, Universidade de Lisboa, Portugal
[u] Department of Neurosciences, Psychology, Drug Research and Child Health (NEUROFARBA), University of Florence, Florence, Italy
[v] IRCCS Don Gnocchi, Firenze, Italy

ARTICLE INFO

ABSTRACT

Brain atrophy as measured from structural MR images, is one of the primary imaging biomarkers used to track neurodegenerative disease progression. In diseases such as frontotemporal dementia or Alzheimer's disease, atrophy can be observed in key brain structures years before any clinical symptoms are present. Atrophy is most commonly captured as volume change of key structures and the shape changes of these structures are typically not analysed despite being potentially more sensitive than summary volume statistics over the entire structure.

In this paper we propose a spatiotemporal analysis pipeline based on Large Diffeomorphic Deformation Metric Mapping (LDDMM) to detect shape changes from volumetric MRI scans. We applied our framework to a cohort of individuals with genetic variants of frontotemporal dementia and healthy controls from the Genetic FTD Initiative (GENFI) study. Our method, take full advantage of the LDDMM framework, and relies on the creation of a population specific average spatiotemporal trajectory of a relevant brain structure of interest, the thalamus in our

* Corresponding author. VISAGES team, IRISA-Inria Bretagne Atlantique, Rennes, France.
  E-mail address: claire.cury.pro@gmail.com (C. Cury).
[1] List of consortium members in appendix.

case. The residuals from each patient data to the average spatiotemporal trajectory are then clustered and studied to assess when presymptomatic mutation carriers differ from healthy control subjects.

We found statistical differences in shape in the anterior region of the thalamus at least five years before the mutation carrier subjects develop any clinical symptoms. This region of the thalamus has been shown to be predominantly connected to the frontal lobe, consistent with the pattern of cortical atrophy seen in the disease.

1. Introduction

Neurodegenerative diseases such as frontotemporal dementia (FTD) present progressive symptoms of behavioural and cognitive dysfunction. These changes follow many years of a clinically silent phase in the disease, where abnormal proteins slowly accumulates within the brain, leading to neurodegenerative processes that ultimately result in loss of function. Reliably identifying presymptomatic changes in individuals could lead to intervention with therapies that could slow, or even halt, the onset of these diseases. However, finding a cohort of presymptomatic individuals guaranteed to develop a form of dementia can be challenging. One common strategy is to investigate people who are at-risk for rare autosomal dominant forms of dementia. Half of these individuals are carriers of the mutation, allowing for comparisons between carriers and non-carriers at various stages within the disease process. In the case of genetic FTD, roughly one third of all cases are caused by autosomal dominant mutations, primarily in three genes: chromosome 9 open reading frame 72 (*C9orf72*), progranulin (*GRN*), and microtubule associated protein tau (*MAPT*) (Rohrer and Warren, 2011). As the name would suggest, in all mutations, there is early involvement of both the frontal and temporal lobes, as well as the insula where differences can be observed as early as ten years before estimated age of expected symptom onset, as shown in Rohrer et al. (2015). However, there are additional structures, such as the thalamus, which also appear to be implicated to some degree early on in the disease process (Bocchetta et al.). In many forms of FTD, clinical presentations suggest a left/right asymmetry in terms of which hemisphere is more affected, and this is often supported by evidence of increased atrophy within the affected hemisphere (Boccardi et al., 2002). However, the affected side is not consistent across all cases, and in some cases, there is no evidence of an asymmetry. As this asymmetry is likely to start early in the disease process, it must be taken into account when looking to detect early changes with any sensitivity.

One biomarker that shows promise during the presymptomatic phase is measurement of atrophy derived from structural magnetic resonance imaging (MRI) (Benzinger et al., 2013; Rohrer et al., 2015; Schott et al., 2010). Volumes summarizing change within a region of interest (ROI) tend to be more sensitive to early change than voxelwise approaches, but they do not provide any spatial localisation as to where the atrophy is occurring within the ROI. Conversely, voxelwise analysis can provide better spatial localisation, but the mass univariate nature of the analysis requires correction for multiple comparisons to control for false positive findings, which often results in reduced sensitivity. As loss of brain volume will imply a change in the shape of the structure, a third option is to perform the shape analysis over time for a structure of interest. This could provide more spatial information than a single summary measure of volume alone, but does not require the same level of multiple comparisons as a voxelwise analyses. Given the decades long nature of the disease process, it is not yet feasible to measure the complete time course within one individual. Therefore, the pattern of atrophy over the course of the disease must be estimated through spatiotemporal regression models based on large populations of either cross-sectional data or through longitudinal data that covers a smaller segment (i.e. a few years) of the disease process within each individual.

There have been numerous approaches to spatiotemporally model trajectories for ageing and dementia. Some methods model this evolution using dense 4D deformation fields to measure change between timepoints. Lorenzi et al. (2010) modelled the 4D deformation fields within a population to obtain subject-specific measurements of atrophy. An extension of this work discriminated spatiotemporal patterns that could be attributed to natural ageing versus those that were related to disease (Lorenzi et al., 2015). Other groups establish point correspondences between subjects on a surface representation, and then apply mixed effects models at those points (Datar et al., 2012; Muralidharan et al., 2014; Younes et al., 2014), providing fixed effects that represent the change across the overall population while allowing individual longitudinal trajectories as random effects. More complex representations of surfaces can be used, as in Durrleman et al. (2013), they proposed a spatiotemporal regression approach to estimate continuous subject-specific trajectories of longitudinal data.

In our previous work (Cury et al., 2016), we defined the shape of the structure of interest as its 3D outline that is rotation and translation invariant. Differences between shapes were quantified using the Large Deformation Diffeomorphic Metric Mapping (LDDMM) framework (Trouvé, 1998; Beg et al., 2005; Glaunès et al., 2008), producing a smooth and invertible continuum between all possible shapes within the population. The smooth representation of these deformations also acted as low-pass filter, reducing the effects of irregularities and errors in the surface boundaries. Overall, our approach consisted of three main steps. First, using all available data, we compute an average shape spatiotemporal trajectory. Second, for every individual shape we evaluate its distance from the mean trajectory. Last, after spatially normalising all the subject-specific distances to the mean, we run a statistical analysis on the subject-specific residuals to assess when a shape starts diverging from normality. This previous work presented a global spatio-temporal analysis, on one side of the brain, without considering a potential left/right asymmetry of the disease. In this paper, we build on the aforementioned framework, which we altered in two main ways. First, we take into consideration the potential asymmetry of FTD by considering the left and right structures using a common shape representation. Second, we modified our feature extraction method using a clustering approach to ensure we can attribute the recovered differences to substructure of the shape under study, and made a novel local analysis, based on clustering of deformations, which takes better advantage of the LDDMM framework.

We apply this approach to data from the Genetic FTD Initiative (GENFI), an international study of autosomal dominant forms of FTD aimed at collecting multimodal neuroimaging, alongside other biomarkers with the objective of obtaining an improved understanding of the changes that are occurring during the presymptomatic phase of the disease. In general, the expected age of onset of clinical symptoms is estimated by using the average age of onset in the family of the subject, allowing to align the different subjects onto a single time axis. We applied our method to a subcortical structure, the thalamus, which has been shown to present volumetric differences before onset in Rohrer et al. (2015). We used the expected age to onset to characterise the time progression. In the next section, we will present the different steps of the proposed framework before then further describing the experiment and associated results.

2. Method

We indicate with $\{(S_i, t_i)\}_{i \in \{0; ...; N-1\}}$ a set of *N* shapes associated with a corresponding time point t_i. With analogy to classical random-effect-modelling approaches, we assume that each shape is a random realisation of a common underlying spatiotemporal process $\phi(t)$:

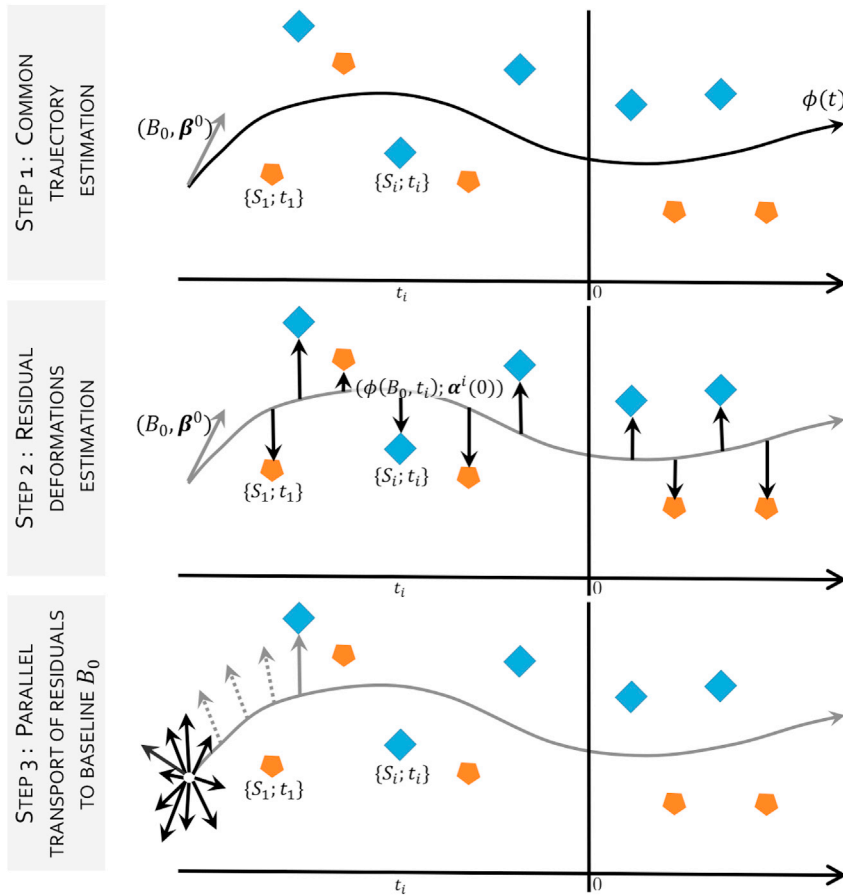$$S_i = \rho_i(\phi(B_0, t_i)) + \varepsilon_i,$$

Fig. 1. Overview of the proposed regression approach. The temporal axis indicates the time variable attached to the data, in this case the estimated years to expected symptom onset. The residual deformations (step 2) ρ_i parametrised by ($\phi(B_0, t_i); \boldsymbol{\alpha}^i(0)$) computed from the common trajectory (step 1) ϕ parametrised by ($B_0; \boldsymbol{\beta}^0$), cannot be analysed because they are defined on different spaces i.e. $\phi(B_0, t_i)$. They have to be transported to a common space (i.e. B_0) along the geodesic ϕ, so they can be analysed (step 3).

where B_0 is a common reference frame, and ρ_i is a subject-specific "residual" deformation accounting for individual deviation from the mean shape. We characterise this residual through the diffeomorphism linking the shape S_i to the corresponding sample of the common spatiotemporal trajectory at time point t_i. We also assume that ε_i is Gaussian randomly distributed noise. In order to identify group-wise differences between the given populations, we rely on the analysis of the subjects-specific residuals deformations ρ_i.

This is a challenging problem, since all ρ_i are defined at different time points along the common spatiotemporal trajectory, and therefore cannot be directly compared in a common anatomical framework. Moreover, the optimisation of the functional for the simultaneous estimation of the group-wise trajectory and random effects is not trivial, and would ultimately result in expensive and thus impractical numerical schemes. For these reasons, we propose a serial optimisation of the problem by introducing an efficient numerical framework composed of three steps illustrated in Fig. 1.

(i) First, we assume that the residuals deformations ρ_i are fixed, and we estimate the common trajectory $\phi(t)$. (ii) Second, given the modelled trajectory ϕ, we estimate the residuals deformations ρ_i through non-linear registration between the trajectory point $\phi(B_0, t_i)$ and S_i. (iii) Third, we spatially normalise the residual deformations in the common initial reference space B_0 using parallel transport.

The proposed framework relies on the mathematical setting of the Large Diffeomorphic Deformation Metric Mapping (LDDMM) framework and the varifold representation of shapes (section 2.1). This choice allows a mathematically consistent definition of all steps (section 2.2), namely: (i) the spatiotemporal regression, (ii) the ρ_i deformations estimation, and (iii) the normalisation of the initial momentum of ρ_i through parallel transport.

2.1. Large diffeomorphic deformation metric mapping and varifold representation

The LDDMM framework (Trouvé, 1998; Beg et al., 2005) is a mathematical and algorithmic framework based on flows of diffeomorphisms, which allows comparing anatomical shapes as well as performing statistics. The framework used in this paper is a discrete parametrisation of the LDDMM framework, as proposed by Durrleman et al. (2011), based on a finite set of N_{B_0} control points overlaid on the 3D space enclosing the initial shape B_0. The control points number and position are independent from the shapes being deformed as they do not require to be aligned with the shapes' vertices. They are used to define a potentially infinite-dimensional basis for the parametrization of the deformation. Momentum vectors are associated with the control points and are used as weights for the decomposition of a given deformation onto this basis.

Deformation maps $\varphi_v : \mathbb{R}^3 \rightarrow \mathbb{R}^3$ are built by integrating time-varying vector fields $(v_t)_{0 \leq t \leq 1}$, such that each $v(\cdot, t)$ belongs to a Reproducing Kernel Hilbert Space (RKHS) V with kernel K_V. We use a Gaussian kernel for all control points x, y:

$$k_V(x, y) = \exp\left(\frac{-|x - y|^2}{\lambda^2}\right) \mathrm{Id},$$

with Id the identity matrix, and λ a scale factor which determines the size of the kernel and therefore the degree of smoothness of the deformations. We define $\varphi_v(x) = \phi_v(x, 1)$ as the diffeomorphism induced by $v(x, t)$ where $\phi_v(x, 1)$ is the unique solution of the differential equation:

$$\frac{d\phi_v}{dt}(x, t) = v(\phi_v(x, t), t), \forall t \in [0, 1] \quad \text{with} \quad \phi_v(x, 0) = x, \forall x \in \mathbb{R}^3.$$

Velocity fields $v(\cdot, t)$ are controlled via an energy functional $\int_0^1 \| v(\cdot,$

$t)\|_V^2 dt$, where $\|\cdot\|_V$ is a Hilbert norm defined on vector fields of $\mathbb{R}^3$, which is used as a regularity term in the matching functional to penalise non-regularity. In the LDDMM framework, matching two shapes S and T requires estimating an optimal deformation map $\phi : \mathbb{R}^3 \to \mathbb{R}^3$ such that $\phi(S)$ is close to T. This is achieved by optimising

$$d([\varphi_v(S)], [T])^2 + \gamma \int_0^1 \| v(\cdot, t) \|_V^2 \, dt,$$

where γ balances the regularity of ϕ_v against the spatial proximity d, a similarity measure between the varifold representation of $\varphi_v(S)$ and T noted respectively $[\varphi_v(S)]$ and $[T]$.

In a discrete setting, the vector fields $v(x, t)$ corresponding to optimal maps are expressed as combinations of spline parametrised fields that involve the reproducing kernel K_V of the space V:

$$v(x, t) = \sum_{p=1}^{N_{B_0}} K_V(x, x_p(t)) \alpha_p(t),$$

where $x_p(t) = \phi_v(x_p, t)$ are the trajectories of control points x_p. The control points are regularly spaced on a 3D grid overlaid on the space that contains the mesh of the subject S. The control point spacing is defined by the size of the kernel K_V. The time-dependent vectors $\alpha_p(t) \in \mathbb{R}^3$ are referred to as momentum vectors attached to x_p. The full deformation can be encoded by the set of initial momentum vectors $\alpha(0) = \{\alpha_p(0)\}_{1 \leq p \leq n}$ located at the points $\{x_p\}_{1 \leq p \leq n}$. This allows the analysis of a set of deformation maps from a given template to the observed shapes by performing statistics on the initial momentum vectors defined on control points located around the template shape. The process of generating back any deformation map from initial conditions $(x_p(0), \alpha_p(0))$, i.e. integrating the geodesic equations, is called geodesic shooting or exponential map and is noted $\exp_{x_p(0)}(\alpha_p(0))$.

As previously stated, varifolds are used to represent shapes (Charon and Trouvé, 2013). They are non-oriented versions of the representation with currents (Vaillant et al., 2005), which are used to efficiently model a large range of shapes. To represent a shape S as a varifold, the shape space is embedded into the dual space of a RKHS W, noted W^*, and encoded using a set of non-oriented unit normals attached on each vertex of the shape. This kernel-based embedding allows to define a distance between different embedded shapes. Varifolds are robust to varying topologies, do not require point to point correspondences, and embed the shapes in a vector space, which facilitate the interpretation of results. The varifold representation of a discretised mesh composed by M triangles S is noted $[S]$ and writes: $[S](\omega) = \sum_{k=1}^M \omega(c_k) \tau(c_k)^2 / \|\tau(c_k)\|$ with ω a vector field in W, c_k the centre of the triangle k, and $\tau(c_k)$ the tangent of the surface S at point c_k.

2.2. Residual extraction framework

Due to the asymmetry of the disease, the proposed framework has been designed so that it is unbiased to the affected side. For each subject, rather than considering the left or right structure, we build a mean shape by averaging both sides. First, the structure of interest is segmented using the method proposed by Cardoso et al. (2013). Second, we flip all input T1w brain images and segmentation masks, in order to have all structures, left and right, on the same side. Third, we affinely align the T1w brain images (the originals and the flipped ones) to a subject-specific mid-space (Modat et al., 2014). The MNI52 atlas was used to define the mid-space and ensure that all subjects have a similar total intra-cranial volume (TIV). TIV varies from subject to subject due to normal variability in the population. Alignment to a common mid-space enables to discard this inter-subject variability through normalisation. The obtained affine transformations are then applied to the corresponding segmentation masks. Fourth, we compute a mask covering the area of the structure of interest and its surroundings for all T1w MRI, to

estimate a rigid refinement focused on the area of interest. This is achieved by a 6-voxel dilation of the union of all propagated masks to ensure that for each subject, the structure of interest and its surrounding are considered. The rigid refinement step is done using the T1w MRIs rather than the segmented shape. Finally, we extract the meshes of the left (flipped, L_i) and right structures (R_i), and compute the mean shape, by estimating the diffeomorphisms $\chi_v^{(i)}$ for each subject i, such as $\chi_v^{(i)} = argmin \frac{1}{2} (\| [\chi_{v_i}(L_i)] - [S_i] \|_{W^*}^2 + \| [\chi_{v_i}(R_i)] - [S_i] \|_{W^*}^2) + \gamma \int_0^1 \| v_i(\cdot, t) \|_V^2 \, dt$ with W^* the space of varifolds and S_i, the obtained subject-specific average shape of the structure of interest, is associated with a temporal information t_i, the number of years to the expected onset (EYO) of the subject i.

The computation of the spatiotemporal regression (Durrleman et al., 2013) requires an initial shape $B_0 = \{x_p\}_{p=1,...,N_{B_0}}$ as reference. To avoid any bias towards a subject selected as the initial shape, we estimate the initial shape from the 10 subjects who are the furthest away from expected symptom onset, who are all approximately 40 years before their expected onset of clinical symptoms according to EYO. We estimate the centroid of those 10 subjects using the diffeomorphic Iterative Centroid method (Cury et al., 2014), which estimates a centre of a given population in a reasonable computation time (Cury et al., 2018).

The spatiotemporal regression of the set of shapes $\{(S_i, t_i)\}_{i \in \{0;...;N-1\}}$ is implemented in the Deformetrica software (Durrleman et al., 2014; Routier et al., 2014).[2] The EYO values are discretised into T time points. Starting from B_0 at time $t = 0$, a geodesic moving through the positions $\phi(B_0, t)$, $\forall t \in \{0; ...; T\}$ is computed by minimising the discrepancy between the model at time t (i.e. $\phi(B_0, t)$) and the observed shapes S_i:

$$E(\phi_v) = \sum_{t_i} d([\phi_v(B_0, t_i)], [S_i])^2 + \gamma \|v\|_{V^\phi}^2,$$

with v the time-varying velocity vector field that belongs to the RKHS V determined by the Gaussian Kernel K_V. The initial momentum vectors $\beta^0(0) = \{\beta_p^0(0)\}_{1 \leq p \leq N_{B_0}}$ are defined on the control points grid overlaid on the baseline shape B_0 and fully encode the geodesic regression parametrised by $\{B_0; \beta^0(0)\}$.

We then compute the residuals diffeomorphic deformations ρ_i between every observation and the spatio-temporal average shape by estimating a geodesic between $\phi(B_0, t_i)$ and $\{S_i, t_i\}$. This yields a set of trajectories parametrised by $\{\phi(B_0, t_i); \alpha^i(0)\}_{i \in \{0;...;N-1\}}$ that encode the deformations ρ_i from the spatio-temporal regression to all subjects, with $\alpha^i(0)$ the initial momentum vectors, where the varying parameter is the step of the deformation. This parameter should not be confused with the time variable corresponding to the EYO and to the time varying deformation of the main spatio-temporal trajectory.

In order to be able to compare this set of momenta, we gather them in the same Euclidean space. This is achieved by transporting all momenta into the initial space of $B_0 = \phi(B_0, 0)$, using a parallel transport method based on Jacobi fields as introduced in (Younes, 2007). Parallel transporting a vector along a curve (the computed trajectory parametrised by $(B_0; \beta^0(0))$) consists in translating it across the tangent spaces along the curve by preserving its parallelism, according to a given connection. The Levi-Civita connection is used in the LDDMM framework. The vector is parallel transported along the curve if the connection is null for all steps along the curve (Lorenzi and Pennec, 2013). We use Jacobi field instead of the Schild's Ladder method (Kheyfets et al., 2000), to avoid the cumulative errors and the excessive computation time due to the computation of Riemannian Logarithms in the LDDMM framework, required for the Schild's Ladder. The cumulative errors would have differed from subject to subject and thus introduce a bias. Indeed, their distances from the baseline shape vary, as they all are at different points along the

---

[2] http://www.deformetrica.org/.

temporal axis. The Jacobi field, used to transport a vector $\boldsymbol{\alpha}^i(0)$ from a time t to the time $t_0 = 0$ along the geodesic γ, is defined as:

$$J_{\gamma(t)}\big(0, -\boldsymbol{\beta}^0(t), \boldsymbol{\alpha}_i(0)\big) = \frac{\partial}{\partial \varepsilon} \exp_{\gamma(t)}\big(1/T\big(-\boldsymbol{\beta}^0(t) + \varepsilon \boldsymbol{\alpha}_i(0)\big)\big).$$

The transported initial momentum vector $\boldsymbol{\alpha}_i(0)$ is noted $\boldsymbol{\theta}_i(0)$. After parallel transporting all residuals, all initial momentum vectors are defined in B_0.

2.3. Feature extraction for statistical analysis

Each transported initial momentum vectors $\boldsymbol{\theta}_i(0)$ is of size $3 \times N_{B_0}$, where N_{B_0} is the number of control point used to parametrise the geodesics.

Jacobian determinants are a geometric measure derived from the full deformation tensor that is commonly used to study shrinkage or growth of the surface. In this work we propose an analysis framework where we decouple the amplitude and the orientation of the deformation. Such an approach will still analyse growth and shrinkage, but also other geometric aspects, such as rotation and torsion, that are not captured by the surface Jacobian. Furthermore, the changes being analysed are residual deformations, which are defined using a purely geometrical spatio-temporal regression. As such, the shape differences that we aim to detect are not necessarily limited to shrinkage or growth, but can be induced by more complex effects.

To analyse direct measures from deformation and to avoid losing statistical power from doing a large number of comparisons, we propose an original clustering approach by grouping the parametrisation (B_0; $\boldsymbol{\beta}^0(0)$) of the spatio-temporal regression ϕ into clusters.

To do so, we defined a similarity measure derived from the positions of the control points x_p, the pairwise angles and the magnitudes of the initial momentum vectors $\{\boldsymbol{\beta}_p^0(0)\}_{1 \leq p \leq N_{B_0}}$ attached to the control point x_p. The difference between two control points x_p and x_q $\forall p, q \in \{1; ...; N_{B_0}\}$ is defined by the euclidean distance, the angle between two vectors is defined by the cosine. The similarity between p and q is defined by $s(p, q) = -5 \|x_p - x_q\|^2 + 2(cos(\beta_p^0, \beta_q^0) + 1) - \left|\|\beta_p^0\|^2 - \|\beta_q^0\|^2\right|$. Parameters are chosen to balance between vector similarity and control point positions and depend on the distance in mm between two points. The distance is determined by the kernel K_V so that clusters encompass control points and their momentum vectors within the same area and look alike. To estimate those clusters, we used a spectral clustering method (von Luxburg, 2007) using the discretisation approach presented in (Jianbo et al., 2003) for initialisation, as it has been shown to be more stable than other approaches such as k-means for initialisation. 3000 different initialisations are generated and we select the best one in term of inertia for spectral clustering. We chose 10 clusters as thought this would be a good balance between reducing the number of multiple comparisons while maintaining some spatial specificity in the analyses and equitable clusters. A mean vector is then computed from the parallel transported residuals defined on the control points of the cluster. This is done for each cluster and for each subject. We then obtain N vectors $\{\nu_{i,k}\}$ per cluster k, and 10 vectors per subject i.

For the statistical analysis, we will use two uncorrelated descriptors for the vectors $\{\nu_{i,k}\}$: the amplitude and the orientation. The orientation of the vectors $\{\nu_{i,k}\}$ is originally represented by 3 angles, one per axis. The angles are then projected via a Principal Component Analysis onto the first eigenvector, therefore the orientation of $\{\nu_{i,k}\}$ considered here is represented by one continuous scalar, leading to the set of responsive variables $\{O_{i,k}\}$.

3. Data and application

As previously mentioned, we applied the proposed framework to the GENFI study and used the thalamus as structure of interest.

Table 1
Data demographics, in absolute values.

	Non-carriers n = 98	Mutation carriers n = 113
Males	59	56
Asymptomatic	98	76
Age in years (med (IQR))	50.2 (62.1–36.6 = 25.5)	52.7 (62.7–41.1 = 21.6)
Years from expected onset:		
$\leq -20 years$	30	21
$-20 \leq years \leq -10$	16	21
$-10 \leq years < 0$	23	22
$0 \leq years$	29	49

3.1. Dataset description

All participants included in this study come from the data freeze 1 of the GENFI cohort described in detail in (Rohrer et al., 2015). Initial results from this cohort (Rohrer et al., 2015) show volumetric differences in the thalamus at least 5 years before expected age of onset with an effect in all genetic subtypes, and so we chose this well-defined subcortical structure for further analysis. In this paper we used 211 participants, 113 mutation carriers (MAPT = 26, GRN = 53, C9ORF = 34) and 98 non-carriers. All participants have a T1-weighted (T1w) MRI available and an associated expected years to symptom onset (EYO). The EYO, ranging from -40 years to $+20$ years, is calculated as the difference between the age of the participant at the time of the T1w acquisition and the mean age at onset of affected family members, as in (Rohrer et al., 2015). The median of the age at onset of all subjects is 59.7 years with inter-quartile range $IQR = 60.5 - 55$. Table 1 shows the demographics of the study participants used in this analysis.

3.2. Application to the thalamus

As previously mentioned in section 2.2, all T1w MRIs and associated segmentations of the structure of interest, the thalamus, are first aligned to a common space. This enables to normalise for intra-cranial volume differences across subjects. We then extracted the meshes corresponding to the thalamus, composed by around 2, 300 vertices. This resulted in 211 thalamus meshes, representing the mean left and the right shape. Each were associated with the EYO of the corresponding subject as well as mutation status: non-carrier and mutation carrier (MC). For the spatio-temporal regression, we used 30 time points, which corresponds approximately to one time point every two years. The space of deformations V was defined using a 11 mm width kernel, approximately half of the length of the thalamus, which leads to a set of 288 control points. For the space of varifolds we used a 5 mm width kernel which covers the size of 2 voxels. This parameter was fixed and thought to be a good compromise between the capture of high frequency changes and the robustness of the approach to noise in the shape segmentation.

Similarly to the volumetric analysis performed by Rohrer et al. (2015), we used a mixed effect model to study the shape difference between the non-carriers and mutation carriers. Amplitude $\{|\nu_{i,k}|\}$ and orientation $\{O_{i,k}\}$ were used as responsive variables and the fixed effects predictors of interest were mutation carrier status, EYO, interaction between mutation carrier status and EYO, sex and the site in which the subject has been scanned. A random intercept for family allows values of the marker to be correlated between family members. Correcting for age of subjects is not relevant here, since there is a strong correlation ($r = 0.9$) between EYO and age.

We performed a Wald test for every model, assessing the difference between the mutation carrier group and the non-carrier group, and the evolution of differences across time. For each analysis with statistically significant differences between both groups, further Wald tests were conducted every 5 years as in the volumetric analysis (Rohrer et al., 2015) to assess how long before the expected onset we could detect changes between mutation carriers and controls.

Table 2
p-values with the corresponding χ^2 value, resulting from the Wald tests testing the mutation carrier (MC) differences (test T1), and the evolution of those differences along time (test T2), for the amplitude of the initial momentum vector and its orientation, for the clusters showing at least one significant test. Bold p-values: ≤ 0.05, and starred (*) p-values indicate the corrected threshold for multiple comparisons: $\leq 2.5e{-}3$.

		C1	C2	C4	C6	C7
Ampl.	T1	$p = 0.48$	$p = 0.51$	$p = \mathbf{1.5e\text{-}3}$ (*)	$p = 0.08$	$p = 0.76$
		$\chi^2_{df=2} = 1.43$	$\chi^2_{df=2} = 1.35$	$\chi^2_{df=2} = 12.94$	$\chi^2_{df=2} = 5.10$	$\chi^2_{df=2} = 0.55$
	T2	$p = 0.24$	$p = 0.26$	$p = \mathbf{1.5e\text{-}3}$ (*)	$p = \mathbf{0.04}$	$p = 0.68$
		$\chi^2_{df=1} = 1.37$	$\chi^2_{df=1} = 1.28$	$\chi^2_{df=1} = 10.08$	$\chi^2_{df=1} = 4.20$	$\chi^2_{df=1} = 0.17$
Orient.	T1	$p = \mathbf{2e\text{-}4}$ (*)	$p = 0.12$	$p = 0.85$	$p = 0.63$	$p = 0.08$
		$\chi^2_{df=2} = 16.60$	$\chi^2_{df=2} = 4.17$	$\chi^2_{df=2} = 0.33$	$\chi^2_{df=2} = 0.92$	$\chi^2_{df=2} = 5.06$
	T2	$p = \mathbf{9e\text{-}4}$ (*)	$p = \mathbf{0.05}$	$p = 0.62$	$p = 0.34$	$p = \mathbf{0.04}$
		$\chi^2_{df=1} = 11.01$	$\chi^2_{df=1} = 3.85$	$\chi^2_{df=1} = 0.25$	$\chi^2_{df=1} = 0.91$	$\chi^2_{df=1} = 4.29$

4. Results

Results for the amplitude and the orientation of the residual momentum vectors are presented in Table 2. We found significant differences, after correction for multiple comparisons, in cluster 1 and cluster 4, for both tests; T1:differences between MC and controls and T2: differences over time between MC and controls. Those differences are significant after Bonferroni correction for multiple comparisons (20 tests). Cluster 1 shows differences in the orientation, and no differences in the amplitude, whereas cluster 4 shows significant differences for those 2 tests in amplitude, and no differences in orientation. Those 2 clusters are thus selected for the next Wald test step. Wald tests were conducted every 5 years between 20 years before the expected onset and 10 years after the expected onset to limit the number of tests, since we would not expect substantial changes in volume or shape 20 years before onset. Results are shown in Fig. 2, the p-values and confidence intervals are corrected for multiple comparison across time using Bonferroni correction.

The orientation of the cluster 1 deformation shows significant differences between the mutation carriers and controls, 5 years before EYO ($p = 0.03$), the uncorrected for this cluster is $p = 2e{-}3$, to keep a head to head comparison with the previous studies on this dataset (Rohrer et al.,

2015; Cury et al., 2016) in which the p-values at -5 EYO was significant but higher than here. The uncorrected p-values show significant differences at 10 years before EYO, with $p = 0.048$ for the orientation of cluster 1. The amplitude between the two groups doesn't differ significantly for the cluster 4 before EYO for corrected p-values, and differs 5 years before onset without correction ($p = 0.05$). Fig. 3 shows the initial momentum vectors of clusters 1 and 4, and the amount of displacement due to the deformations corresponding to those clusters 1 and 4, where each cluster has its own colour scale, since the maximum displacement for cluster 4 is about 3 mm, against 9 mm for cluster 1. Deformations affect more the anterior part of the thalamus.

Since the number of clusters used (i.e. 10), is an arbitrary choice, we tried to reproduce the results with different number of clusters. We performed the analysis for 2, 4, 6, 8, 10, 12, 14 and 16 clusters which results can be found in supplementary material (https://zenodo.org/record/1324234). For 6 clusters and 16 clusters, there were differences in orientation for one of the clusters which deformation corresponds to the one of cluster 1 (see Fig. 3). From 8 clusters to 14 clusters, we found a cluster with strong differences 5 years before the expected onset ($p < 0.01$) in orientation whose deformation corresponds again to the one of the cluster 1 ($p = 0.003$). The change in orientation for the deformation recovered within cluster 1 (see Fig. 3) appears to be stable for different clustering of the parametrisation of the global spatiotemporal trajectory (https://zenodo.org/record/1324234, Fig. 1).

5. Discussion and conclusion

We applied a novel method of statistical shape analysis to a cohort of individuals with genetic FTD in order to localise any presymptomatic differences present in the shape of the thalamus. From the analysis, we conclude that differences are observed five years before expected symptom onset. While volumetric analysis (Rohrer et al., 2015) and our initial shape analysis (Cury et al., 2016) also found these changes, this method showed significance that survived correction for multiple comparisons. The change in shape is primarily attributable to differences in orientation of the deformation rather than changes in amplitude of the deformation, which would imply a simple scaling effect of the region. This result confirms our previous shape analysis in this cohort (Cury et al., 2016) that was performed at a global level through a kernel principal component analysis. The first mode of variation which detected significant shape differences around the same point with respect to EYO did not capture volume differences but only changes in the orientation of the deformation. The results of those studies seem to indicate that shape changes occur before volume changes.
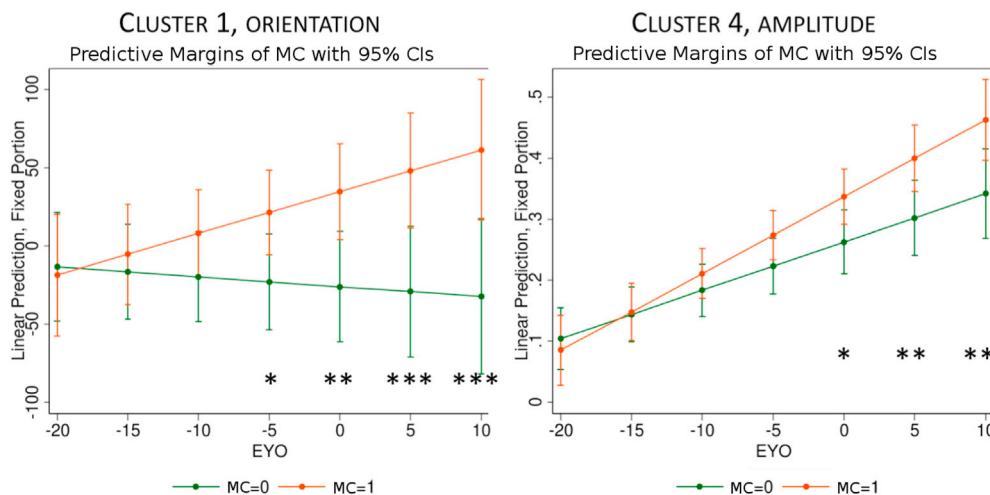

Fig. 2. Cluster 1 (orientation component) and cluster 4 (amplitude component) estimates in mutation carriers and controls, by estimated time from expected symptoms onset (EYO). p-values and confident interval are Bonferroni corrected. *: $p < 0.05$, **: $p < 0.01$, ***: $p < 0.001$.
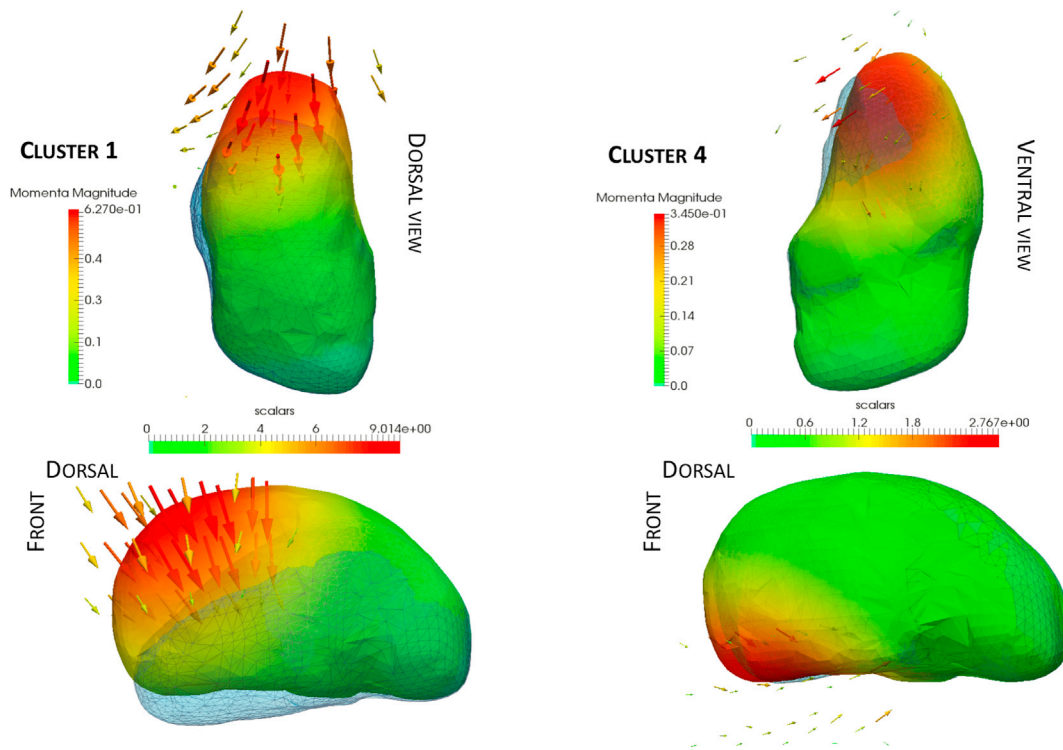
Fig. 3. Deformation obtained by the momentum vectors (displayed here and coloured by amplitude) of Cluster 1 and Cluster 4. The colour map is in millimetres and indicates the displacement due to the corresponding deformation (blue meshes). The scale for Cluster 1 range from 0 mm to 9 mm, and from 0 mm to 2.8 mm for Cluster 4.
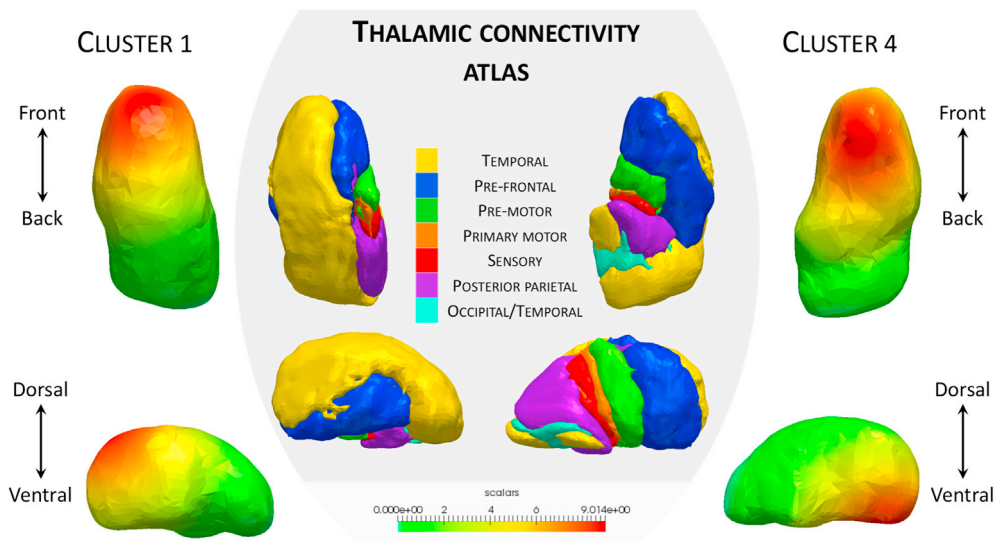

Fig. 4. Thalamic connectivity atlas, and deformations clusters 1 and 4. The orientation of cluster 1 leads to significant differences between MC and controls 5 years before EYO.

The regions of the thalamus most affected in the analysis are anterior, overlapping with the anterior nuclei group. The main connections of these nuclei are to the prefrontal cortices, an area universally affected in all genetic forms of FTD. To illustrate this purpose, we used the Oxford thalamic connectivity atlas, a thalamic atlas based on its anatomical connectivity to the cerebral cortex (Behrens et al., 2003), and displayed at Fig. 4 the atlas next to the clusters 1 and 4.

Whilst differences are seen in cortical involvement within the different genetic forms of FTD (Cash et al., 2018), it may well be that this joint analysis of GRN, C9orf72 and MAPT mutations is only identifying thalamic regions jointly affected.

This approach could also be used to explore other regions known to be implicated in FTD, such as the insular cortex, which is located in the lateral sulci and is connected to the limbic system, and to the thalamus. In fact, it would be interesting to analyse the insula and thalamus together, and the insula only, so we could investigate if shape changes in both structures are linked.

The small numbers in each group precluded any analysis of the

individual genetic types, but it will be important to investigate future data freezes from the GENFI study with larger numbers, particularly the C9orf72 group who have been shown to have early thalamic involvement (Cash et al., 2018).

Future studies should also evaluate the initial momentum vectors of individual geodesic evolution of shapes from each subject, through longitudinal data. Those individual evolutions would provide information on the differences of evolutions of shape between the mutation carriers and the controls.

Acknowledgements

Appendix A. Supplementary data

Supplementary data to this article can be found online at https://doi.org/10.1016/j.neuroimage.2018.11.063.

References

Beg, M.F., Miller, M.I., Trouvé, A., Younes, L., 2005. Computing large deformation metric mappings via geodesic flows of diffeomorphisms. Int. J. Comput. Vis. 61 (2), 139–157.

Behrens, T.E.J., Johansen-Berg, H., Woolrich, M.W., Smith, S.M., Wheeler-Kingshott, C. a. M., Boulby, P.A., Barker, G.J., Sillery, E.L., Sheehan, K., Ciccarelli, O., Thompson, A.J., Brady, J.M., Matthews, P.M., 2003. Non-invasive mapping of connections between human thalamus and cortex using diffusion imaging. Nat. Neurosci. 6 (7), 750–757. https://doi.org/10.1038/nn1075.

Benzinger, T.L.S., Blazey, T., Jack, C.R., et al., 2013. Regional variability of imaging biomarkers in autosomal dominant Alzheimer's disease. Proc. Natl. Acad. Sci. Unit. States Am. 110 (47), E4502–9.

Boccardi, M., Bresciani, L., Geroldi, C., Beltramello, A., Frisoni, G.B., Laakso, M.P., 2002. Clinical characteristics of frontotemporal patients with symmetric brain atrophy. Eur. Arch. Psychiatr. Clin. Neurosci. 252 (5), 235–239. https://doi.org/10.1007/s00406-002-0388-z.

Bocchetta, M., Gordon, E., Cardoso, M.J., Modat, M., Ourselin, S., Warren, J.D., Rohrer, J.D., 2018. Thalamic atrophy in frontotemporal dementia - not just a C9orf72 problem. Neuroimage Clin. 18, 675–681.

Cardoso, M.J., Leung, K., Modat, M., Keihaninejad, S., Cash, D., Barnes, J., Fox, N.C., Ourselin, S., for ADNI, 2013. STEPS: similarity and truth estimation for propagated segmentations and its application to hippocampal segmentation and brain parcelation. Med. Image Anal. 17 (6), 671–684.

Cash, D.M., Bocchetta, M., Thomas, D.L., Dick, K.M., van Swieten, J.C., Borroni, B., Galimberti, D., Masellis, M., Tartaglia, M.C., Rowe, J.B., Graff, C., Tagliavini, F., Frisoni, G.B., Laforce, J., Robert, Finger, E., de Mendon?a, A., Sorbi, S., Rossor, M.N., Ourselin, S., Rohrer, J.D., 2018. Patterns of gray matter atrophy in genetic frontotemporal dementia: results from the GENFI study. Neurobiol. Aging 62, 191–196.

Charon, N., Trouvé, A., 2013. The varifold representation of nonoriented shapes for diffeomorphic registration. SIAM J. Imag. Sci. 6 (4), 2547–2580. https://doi.org/10.1137/130918885.

Cury, C., Glaunès, J.A., Colliot, O., 2014. Diffeomorphic iterative centroid methods for template estimation on large datasets. In: Nielsen, F. (Ed.), Geometric Theory of Information, Signals and Communication Technology. Springer International Publishing, pp. 273–299.

Cury, C., Lorenzi, M., Cash, D., Nicholas, J.M., Routier, A., Rohrer, J., Ourselin, S., Durrleman, S., Modat, M., 2016. Spatio-temporal shape analysis of cross-sectional data for detection of early changes in neurodegenerative disease. In: Reuter, M., Wachinger, C., Lombaert, H. (Eds.), Spectral and Shape Analysis in Medical Imaging, vol 10126. Springer International Publishing, pp. 63–75. https://doi.org/10.1007/978-3-319-51237-2_6. http://link.springer.com/10.1007/978-3-319-51237-2_6.

Cury, C., Glaunès, J.A., Toro, R., Chupin, M., Schumann, G., Frouin, V., Poline, J.-B., Colliot, O., 2018. The imagen consortium, statistical shape analysis of large datasets based on diffeomorphic iterative centroids. Front. Neurosci. 12, 803. https://doi.org/10.3389/fnins.2018.00803. https://www.frontiersin.org/article/10.3389/fnins.2018.00803/full.

Datar, M., Muralidharan, P., Kumar, A., Gouttard, S., Piven, J., Gerig, G., Whitaker, R., Fletcher, P.T., 2012. Mixed-effects shape models for estimating longitudinal changes in anatomy. In: Hutchison, D., Kanade, T., Kittler, J., Kleinberg, J.M., Mattern, F., Mitchell, J.C., Naor, M., Nierstrasz, O., Pandu Rangan, C., Steffen, B., Sudan, M., Terzopoulos, D., Tygar, D., Vardi, M.Y., Weikum, G., Durrleman, S., Fletcher, T., Gerig, G., Niethammer, M. (Eds.), Spatio-temporal Image Analysis for Longitudinal and Time-series Image Data, vol 7570. Springer Berlin Heidelberg, Berlin, Heidelberg, pp. 76–87.

Durrleman, S., Prastawa, M., Gerig, G., Joshi, S., 2011. Optimal data-driven sparse parameterization of diffeomorphisms for population analysis. In: Hutchison, D., Kanade, T., Kittler, J., Kleinberg, J.M., Mattern, F., Mitchell, J.C., Naor, M., Nierstrasz, O., Pandu Rangan, C., Steffen, B., Sudan, M., Terzopoulos, D., Tygar, D., Vardi, M.Y., Weikum, G., Sz??kely, G., Hahn, H.K. (Eds.), Information Processing in Medical Imaging, vol 6801. Springer Berlin Heidelberg, Berlin, Heidelberg, pp. 123–134.

Durrleman, S., Pennec, X., Trouvé, A., Braga, J., Gerig, G., Ayache, N., 2013. Toward a comprehensive framework for the spatiotemporal statistical analysis of longitudinal shape datas. Int. J. Comput. Vis. 103 (1), 22–59. https://doi.org/10.1007/s11263-012-0592-x.

Durrleman, S., Prastawa, M., Charon, N., Korenberg, J.R., Joshi, S., Gerig, G., Trouvé, A., 2014. Morphometry of anatomical shape complexes with dense deformations and sparse parameters. Neuroimage 101 (0), 35–49. https://doi.org/10.1016/j.neuroimage.2014.06.043.

Glaunès, J., Qiu, A., Miller, M.I., Younes, L., 2008. Large deformation diffeomorphic metric curve mapping. Int. J. Comput. Vis. 80 (3), 317–336.

Jianbo, S.Y., Yu, S.X., Shi, J., 2003. Multiclass spectral clustering. In: In International Conference on Computer Vision, pp. 313–319.

Kheyfets, A., Miller, W.A., Newton, G.A., 2000. Schild's ladder parallel transport procedure for an arbitrary connection. Int. J. Theor. Phys. 39 (12), 2891–2898. https://doi.org/10.1023/A:1026473418439.

Lorenzi, M., Pennec, X., 2013. Efficient parallel transport of deformations in time series of images: from Schild's to Pole ladder. J. Math. Imag. Vis. 50 (1–2), 5–17.

Lorenzi, M., Ayache, N., Frisoni, G., Pennec, X., et al., 2010. 4D registration of serial brain's MR images: a robust measure of changes applied to Alzheimer's disease. In: MICCAI Workshop, Spatio Temporal Image Analysis Workshop (STIA).

Lorenzi, M., Pennec, X., Frisoni, G.B., Ayache, N., 2015. Disentangling normal aging from Alzheimer's disease in structural magnetic resonance images. Neurobiol. Aging 36, S42–S52. https://doi.org/10.1016/j.neurobiolaging.2014.07.046.

Modat, M., Cash, D.M., Daga, P., Winston, G.P., Duncan, J.S., Ourselin, S., 2014. Global image registration using a symmetric block-matching approach. J. Med. Imag. 1 (2), 024003.

Muralidharan, P., Fishbaugh, J., Johnson, H.J., Durrleman, S., Paulsen, J.S., Gerig, G., Fletcher, P.T., 2014. Diffeomorphic shape trajectories for improved longitudinal segmentation and statistics. In: Golland, P., Hata, N., Barillot, C., Hornegger, J., Howe, R. (Eds.), Medical Image Computing and Computer-assisted Intervention ??? MICCAI 2014, vol 8675. Springer International Publishing, pp. 49–56.

Rohrer, J.D., Warren, J.D., 2011. Phenotypic signatures of genetic frontotemporal dementia. Curr. Opin. Neurol. 24 (6), 542–549. https://doi.org/10.1097/WCO.0b013e32834cd442.

Rohrer, J.D., Nicholas, J.M., Cash, D.M., van Swieten, J., Dopper, E., Jiskoot, L., van Minkelen, R., Rombouts, S.A., Cardoso, M.J., Clegg, S., Espak, M., Mead, S., Thomas, D.L., Vita, E.D., et al., 2015. Presymptomatic cognitive and neuroanatomical changes in genetic frontotemporal dementia in the Genetic Frontotemporal dementia Initiative(GENFI) study: a cross-sectional analysis. Lancet Neurol. 14 (3), 253–262. https://doi.org/10.1016/S1474-4422(14)70324-2.

Routier, A., Gori, P., Fouquier, A.B.G., Lecomte, S., Colliot, O., Durrleman, S., 2014. Evaluation of morphometric descriptors of deep brain structures for the automatic classification of patients with Alzheimer's disease, mild cognitive impairment and elderly controls. In: MICCAI Workshop, Challenge on Computer-aided Diagnosis of Dementia Based on Structural MRI Data.

Schott, J.M., Bartlett, J.W., Fox, N.C., Barnes, J., 2010. Increased brain atrophy rates in cognitively normal older adults with low cerebrospinal fluid Aβ1-42. Ann. Neurol. 68 (6), 825–834. https://doi.org/10.1002/ana.22315. http://www.ncbi.nlm.nih.gov/pubmed/21181717.

Trouvé, A., 1998. Diffeomorphisms groups and pattern matching in image analysis. Int. J. Comput. Vis. 28 (3), 213–221.

Vaillant, M., Glaunès, J., 2005. Surface matching via currents. In: Christensen, G.E., Sonka, M. (Eds.), Information Processing in Medical Imaging, Vol. 3565 of Lecture Notes in Computer Science. Springer Berlin Heidelberg, pp. 381–392.

von Luxburg, U., Nov. 2007. A Tutorial on Spectral Clustering.

Younes, L., 2007. Jacobi fields in groups of diffeomorphisms and applications. Q. Appl. Math. 65, 113–134.

Younes, L., Albert, M., Miller, M.I., Team, B.R., et al., 2014. Inferring changepoint times of medial temporal lobe morphometric change in preclinical alzheimer's disease. Neuroimage: Clinical 5, 178–187.